Journal of the Ceramic Society of Japan 124 [10] 996-1002 2016 Full paper

Combined pyrolysis-ammonolysis treatment to retain C during nitridation of SiBOCN ceramics

Aitana TAMAYO,† Raquel PEÑA-ALONSO,* Maria Alejandra MAZO, Fausto RUBIO and Juan RUBIO

Ceramics and Glass Institute, CSIC, Kelsen 5, 28049 Madrid, Spain
***Siemens AG, Corp Technol, D-81739 Munich, Germany**

Two sets of sol–gel derived glass materials have been prepared and subjected to different thermal treatments. Pyrolysis in inert atmosphere lead to the formation of amorphous Si(B)CO ceramics whereas if the inert atmosphere is changed to NH_3 once the carbon substituents of the preceramic hybrid material transform to a glassy network, the nitrogen is incorporated efficiently while the carbon is retained into the structure, as revealed by ^{29}Si NMR analysis. Raman spectra show a less graphitized structure in the case of B-rich materials because of the reduced mobility of the C atoms due to the formation of mixed (B)CN bonds.

Key-words : Sol–gel, Ammonolysis, FTIR, Silicon-boron carbonitride

[Received April 4, 2016; Accepted July 26, 2016]

1. Introduction

Si-based amorphous polymer-derived ceramics and glasses such as SiC, $Si_xC_yO_z$ or $Si_xC_yN_z$ comprise a family of materials suitable for high temperature applications thanks to their special structural characteristics and stability against crystallization. Tailoring the chemistry of the material in the preceramic state allows incorporating different functionalities in the preceramic polymer that, during the polymer-to-ceramic transformation head the decomposition route towards amorphous or crystalline Si-containing species.[1)–4)] This is the case of boron incorporation in SiOC glasses, that may increase their thermal stability concerning decomposition,[5)] or the SiBCN materials, that possess an improved thermal stability against crystallization compared to SiCN or Si_3N_4 materials.[6)]

The enhanced thermal stability of sol–gel derived SiBCO glasses finds its origin on a phase separation occurring during thermolysis, that may promote the crystallization of β-SiC and the growth of thick nanocrystalline and highly graphitized carbon clusters. Similarly, in C-rich polymer derived SiBCO materials, BC_3 units acts as defects in the crystalline structure leading to the growth of the interfacial region between the silica nanodomains.[7)] The different crystallization processes of B-containing $Si_xC_yO_z$ or $Si_xC_yN_z$ glasses are reported to be based on a three-dimensional diffusion and continuous nucleation controlled growth mechanism. The competitive combination of boron and silicon with carbon may hinder the nucleation of β-SiC, as reported in carborane-polycarbosilane derived ceramics,[8)] but once the nanocrystals appear, the lower viscosity of the SiBOC glasses compared with the B-free SiOC materials favors the mobility of the silicon and carbon atoms and thus the growth of crystalline SiC species.[9)] On the other hand, in SiBCN ceramics obtained via hydroboration of polysilazanes, the formation of a diffusional barrier of BCN inhibits the evolution of the structure towards crystalline phases but, once the crystalline Si_3N_4 appeared, the average crystallite size increases with the boron content[10)] while the graphitization of the free carbon phase is inhibited[11),12)]

The crosslinking degree of the SiBOC materials may be strengthened through the substitution of oxygen by trivalent nitrogen atoms. The ammonolysis treatment is a realizable alternative due to the formation of covalent Si–N bonds and more others reactive species that may undergo further condensation reactions.[13)] This strategy has been successfully employed to synthesize microporous silicon oxycarbonitride ceramics from polycarbosilanes possessing open porosity in the range of ultramicropores, opening the door of new potential application of these materials in the field of gas separation.[14)] Nevertheless, thermolysis of preceramic polymers under a NH_3 atmosphere leads to the elimination of most of the carbon through chemical transformation of Si–H, $Si–CH_3$ and $Si–CH=CH_2$ bonds to imidonitride groups at temperatures probably below 750 K.[13),15)] During ammonolysis, the reaction of NH_3 with the carbon functionalities in the low temperature regime of the polymer-to-ceramic conversion[16)] gives as a result a significant decrease of the carbon content in the final ceramic. The formation of BC_3 and BCN environments are less likely to occur.

In this work we have carried out a combined pyrolysis-ammonolysis treatment instead of a direct ammonolysis treatment in order to minimize the nucleophilic substitution of the organic moieties by NH_2 groups. Since the reaction for the formation of imidonitrile groups is favored when the substituent attached to the Si is the H atom,[15)] we have switched the inert pyrolysis atmosphere to a reactive one (NH_3) at the latest stages of the heat treatment. We will compare the effect of three different pyrolysis routes on two B-containing materials with different carbon contents.

2. Experimental

Tetraethyl orthosilicate, TEOS (ABCR), gamma-aminopropyltriethoxysilane, *γ-APS* (ABCR), triethyl borate, TEB (Merck) and silanol terminated polydimethylsiloxane, PDMS (Mw≈1750, ABCR) were used as primary raw materials, 2-propanol was used as solvent in a constant molar ratio iPrOH/TEOS+TEB = 4.5

† Corresponding author: A. Tamayo; E-mail: aitanath@icv.csic.es
‡ Preface for this article: DOI http://dx.doi.org/10.2109/jcersj2.124.P10-1

DOI http://dx.doi.org/10.2109/jcersj2.16071

whereas distilled water and the catalyst hydrochloric acid were added in a molar ratio to TEOS+TEB equal to 2.5 and 0.15, respectively.

Hybrid materials were prepared through a conventional sol–gel methodology in a three-neck flask thermostatized to 353 K and constant reflux. The reactants were added according to their reactivity. TEOS and PDMS (if used) were added to the flask and left react with the corresponding amounts of H_2O and HCl. TEB was added after 1 h stirring at 600 rpm, and afterwards, the dropwise addition of γ-APS was carried out 5 min before the reaction is finished. The total reaction time was 100 min in all cases.

Two different systems have been explored. The system labelled TA contains TEOS and TEB in a constant weight ratio of 70/30 and the amount of γ-APS varied from 99/1 to 90/10 (as referred to the TEOS+TEB/γ-APS ratio). The system labelled TAP contain TEOS and TEB in a constant weigh ratio fixed at 80/20 and the (TEOS+TEB)/(PDMS+γ-APS) ratio was fixed at 60/40. The alcoxyde γ-APS contribute to the organic fraction of the hybrid preceramic material with its non-hydrolyzable aminopropyl group. The amount of γ-APS varied from 99/1 to 90/10 (TEOS+TEB+PDMS)/γ-APS. In all cases, the obtained samples have been labelled with TA or TAP followed by a number indicative of the relative amount of γ-APS.

Centimeter-size dried hybrid monoliths were subjected to different heat treatments in quartz tubular furnaces under a constant gas flow of the specified composition and a constant heat rate of 2 K/min. Pyrolysis was carried out heating under a constant nitrogen flow fixed at 180 ml/min up to 673, 873, 1073, 1273 and 1373 K with 2 h dwelling at the maximum temperature. Ammonolysis and pyrolysis-ammonolysis treatments have been carried out by using both N_2 and NH_3 gasses conveniently dried and mixed to a NH_3/N_2 molar ratio 3/1 in a glass gas-mixer, to prevent decomposition of NH_3 at high temperature. In both cases, the samples were heated at a constant heating rate of 2 K/min up to 1173 K. After 3 h hours dwelling, the furnace temperature was raised to 1373 K and maintained for 15 h. In the ammonolysis treatment, the specified mixture NH_3/N_2 was flown during all the heat treatment whereas in the combined pyrolysis-ammonolysis treatment N_2 was the only gas used until 1173 K and then, the gas flow was switched to the NH_3/N_2 mixture.

The chemical composition of all the obtained materials was obtained through elemental analysis. The amount of silicon was determined by means of traditional gravimetry whereas for the determination of B, the conventional volumetric methodology was used. Carbon was measured by CO_2 determination passing through an IR cell in the LECO CS-200 equipment. Hydrogen was determined in a Carloerba model EA 1108 Elemental CHNS analyzer and the percentage of nitrogen was measured by means of a differential analyzer N_2/O_2 LECO TC-436. This same equipment provided the relative amount of O in all studied samples.

The materials were characterized by means of infrared spectroscopy in the transmission mode and KBr dilution in a Perkin Elmer Spectrum BX spectrometer. At least 16 scans in the range 4000–400 cm^{-1} were recorded for each sample. Raman spectra were collected under 514 nm laser excitation in a Renishaw InVia Raman spectrometer. ^{29}Si NMR spectroscopy was used for the structural characterization of the obtained materials in a Bruker MSL-400 whose analysis conditions were selected according to the studied nucleus. Spinning rate was fixed to 4 kHz, and the analysis frequency and pulse was 79.5 MHz and 2.5 μs, respectivelly.

Nitrogen adsorption–desorption isotherms were obtained at 77 K in a Tristar 3000 (Micromeritics) after degassing at 423 K for 20 h. Mercury intrusion porosimetry measurements were carried out in a Micrometritics Autopore II 9215 by applying increasing pressures ranged from 0.03 to 412 MPa, allowing the mercury to penetrate within the pores sized from 3 nm to 100 μm. For the determination of the porosity in both the macro and mesopore range, the samples were crushed and sieved. The particles ranged between 1000 and 500 μm were used for the analysis. Helium picnometry was used to determine the real density of the obtained materials by using a Quantachrome Corp Monosorb multipicnometer in samples reduced to powder in an agate mortar and sieved below 50 μm. At least 5 measurements were carried out in each sample and the average value was obtained with a typical error of $\pm$ 0.05 g/cm^3. Real density measurements were carried out in powdered samples, nevertheless both nitrogen adsorption and mercury intrusion porosimetry were carried out in crushed ones.

Hot stage microscopy (HSM) was carried out by using a Leica SPT-M122CE heating stage microscope coupled to a Sony CCD camera. Tests were carried out at a constant heating rate of 7 K/min and inert atmosphere. The HSM curves were obtained from the analysis of the area of pressed powders.

3. Results and discussion

The chemical analysis of the obtained samples shows the main compositional differences between the two studied systems (**Table 1**). The system TA possesses the largest B content and its concentration decreases with increased amounts of γ-APS. The materials in this system also retains a large amount of C after the treatments in NH_3 or in the combined pyrolysis-ammonolysis heat treatment, which in fact also leads to efficient incorporation of both C and N atoms within the structure of the glass samples. Ammonia is known to remove the carbon functionalities in the preceramic polymers through transamination reactions at the very first stages of the polymer-to-ceramic conversion turning the Si–

Table 1. Chemical analysis of the materials obtained with different amounts of g-APS in the preceramic polymer and heat treated in N_2, NH_3 or in a combined N_2/NH_3 treatment

	% APS	N_2	NH_3	N_2/NH_3
TA	1	$SiB_{0.25}O_{2.44}C_{0.19}H_{0.09}$	$SiB_{0.21}O_{2.29}C_{0.29}N_{0.10}H_{0.06}$	$SiB_{0.20}O_{2.19}C_{0.28}N_{0.15}H_{0.05}$
	3	$SiB_{0.23}O_{2.36}C_{0.19}H_{0.08}$	$SiB_{0.20}O_{2.26}C_{0.28}N_{0.07}H_{0.05}$	$SiB_{0.20}O_{2.21}C_{0.26}N_{0.13}H_{0.03}$
	5	$SiB_{0.22}O_{2.28}C_{0.20}H_{0.08}$	$SiB_{0.19}O_{2.25}C_{0.24}N_{0.07}H_{0.03}$	$SiB_{0.19}O_{2.33}C_{0.15}N_{0.06}H_{0.04}$
	7	$SiB_{0.20}O_{2.32}C_{0.20}H_{0.07}$	$SiB_{0.18}O_{2.21}C_{0.25}N_{0.08}H_{0.03}$	$SiB_{0.18}O_{2.22}C_{0.21}N_{0.05}H_{0.03}$
	10	$SiB_{0.20}O_{2.24}C_{0.25}H_{0.06}$	$SiB_{0.17}O_{2.20}C_{0.19}N_{0.08}H_{0.02}$	$SiB_{0.17}O_{2.19}C_{0.18}N_{0.01}H_{0.02}$
TAP	1	$SiB_{0.02}O_{1.58}C_{0.48}H_{0.08}$	$SiB_{0.02}O_{1.61}C_{0.26}N_{0.16}H_{0.01}$	$SiB_{0.02}O_{1.34}C_{0.46}N_{0.52}H_{0.01}$
	3	$SiB_{0.03}O_{1.59}C_{0.47}H_{0.07}$	$SiB_{0.03}O_{1.38}C_{0.31}N_{0.34}H_{0.02}$	$SiB_{0.03}O_{1.20}C_{0.60}N_{0.55}H_{0.02}$
	5	$SiB_{0.03}O_{1.41}C_{0.71}H_{0.11}$	$SiB_{0.02}O_{1.41}C_{0.35}N_{0.25}H_{0.01}$	$SiB_{0.03}O_{1.06}C_{0.73}N_{0.60}H_{0.03}$
	7	$SiB_{0.03}O_{1.45}C_{0.67}H_{0.05}$	$SiB_{0.03}O_{1.40}C_{0.46}N_{0.19}H_{0.03}$	$SiB_{0.04}O_{1.05}C_{0.74}N_{0.59}H_{0.04}$
	10	$SiB_{0.04}O_{1.43}C_{0.71}H_{0.04}$	$SiB_{0.04}O_{1.35}C_{0.50}N_{0.27}H_{0.02}$	$SiB_{0.04}O_{1.25}C_{0.44}N_{0.60}H_{0.02}$

CH_3 moieties into highly reactive NH_2 groups.[16] Nevertheless, the presence of boron may hinder this reaction due to the strong affinity of boron to nitrogen. The higher Lewis acid strength of B^{3+} compared to silicon caused the low-temperature nitridation through breakage of B–O–B linkages.[17] Increasing the amount of γ-APS in the TA system courses with a decrease in the number of B atoms and a minor incorporation of N into the ammonolyzed network whereas in the case of the system TAP, both the N and B content increases with the γ-APS content.

In the combined pyrolysis-ammonolysis treatment, the formation of B–N bonds at low temperature through direct ammonolysis of borosiloxane cannot take place in the absence of NH_3 in the atmosphere and therefore, the incorporation of N decreases compared with the direct ammonolysis especially in the richest γ-APS materials. The low-B-content system TAP reduces significantly the C content after ammonolysis although it incorporates more N than the system TA. The combined N_2/NH_3 treatment leads to the largest retention of C and N incorporation among all the studied samples indicating that in this system, the combined pyrolysis-ammonolysis method is the most effective, at least from the point of view of the chemical composition. The Si–CH_3 moieties contained in the hybrid network may react with the NH_3 atmosphere to form imidonitride bonds which transform into nitrogen-rich silicon derivatives through dehydrocoupling reactions.[18]

The density of the materials from the TA system increases during the pyrolysis treatment showing its maximum at 1073 K. In the ammonolysis treatment, the measured density of the samples is slightly higher than in the pyrolyzed ones reaching the value of 2.2 in the materials containing 10% APS. Similarly, the combined treatment lead to the more densified materials with density values comprised between 2.1 and 2.3 g/cm^3. In the TAP system, the density also increases with the amount of γ-APS and acquires values comprised between 2.0 and 2.4 g/cm^3 either in the pyrolyzed and ammonolyzed materials but remain constant to 2.1 g/cm^3 in the combined heat treatment independently on the amount of γ-APS used during the synthesis. This behavior does not contradict the observed bond density increase in the spectroscopic characterization, as it will be described later. Despite of the fact that both the carbon and nitrogen atoms present larger bonding order than oxygen, this element has higher specific weight and thus, the higher bond density found in the ammonolyzed materials does not necessarily imply higher density than the pyrolyzed ones because the structure is comprised by lighter atoms.

Mercury intrusion porosimetry reveals the macroporous character of all the studied materials. In TA samples, the intrusion curves present a type S curve which is characteristic of bimodal pore size distributions (PSD). This bimodal distribution can be observed in the differential dV/dlogD curves [**Fig. 1**(a)]. This representation allows the identification of two different pore sizes, of around 0.6 and 34 μm. The same PDS was inferred from the analysis of SEM images of the fresh fracture shown in **Fig. 2**. It is appreciated a shift to lower pore sizes in the ammonoyzed TA samples and in the case of the combined treatment, the PSD is centered between the pyrolyzed and ammonolyzed samples, being also the broadest one. In this latter case, the differential pore volume is in between the two other treatments (single pyrolysis or ammonolysis atmosphere). These results are in line with the described density increase of the materials heat treated under NH_3 or in a combined N_2/NH_3; when ammonia is used during heating, a decreased cumulative pore volume is found with respect to the pyrolyzed material.

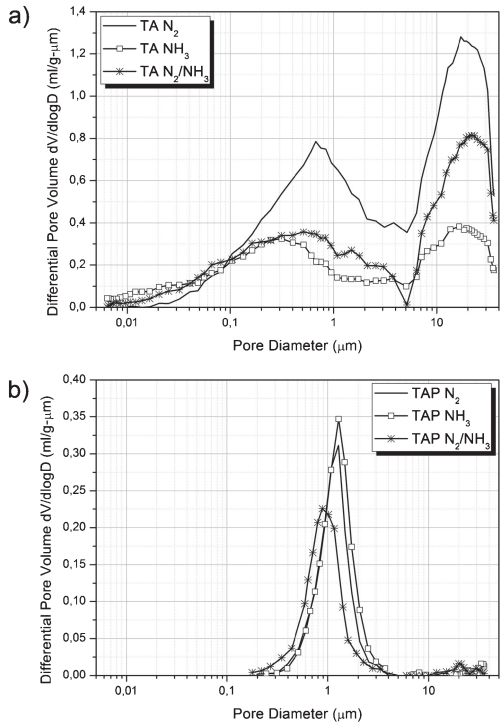

Fig. 1. Pore size distributions obtained from the intrusion branch in Hg mercury intrusion porosimetry of samples with 3% γ-APS from the system a) TA and b) TAP heat treated in different atmospheres.

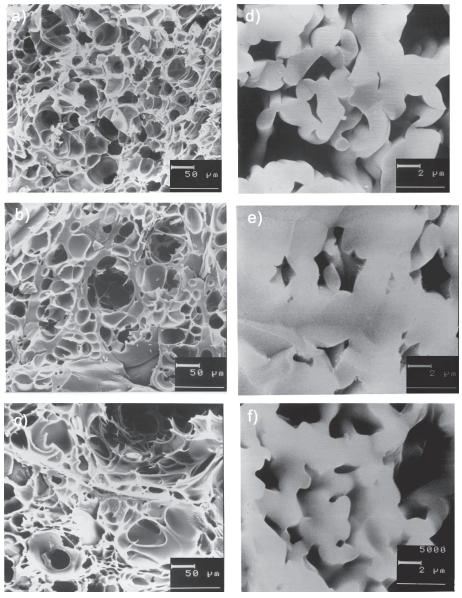

Fig. 2. SEM images of the fresh fracture in samples with 3% γ-APS from the systems TA heat treated in a) N_2, b) NH_3 and c) N_2/NH_3 and from the system TAP heat treated in e) N_2, e) NH_3 and f) N_2/NH_3.

Although mercury intrusion data shown in Fig. 1(a) reveals the existence of pores comprised between 10 and 1000 nm, i.e., some of them still in the high-range detection limit of the N_2 adsorption measurements. Figure 2 present the fresh fracture of the material but, the outer surface (not shown here) revealed a microstructure completely smooth and free of pores (some cracks were visible, possibly due to the release of gasses). Due to the high pressures applied during the mercury intrusion experiments, the pressurized mercury is able to break some of the thin walls of the particles

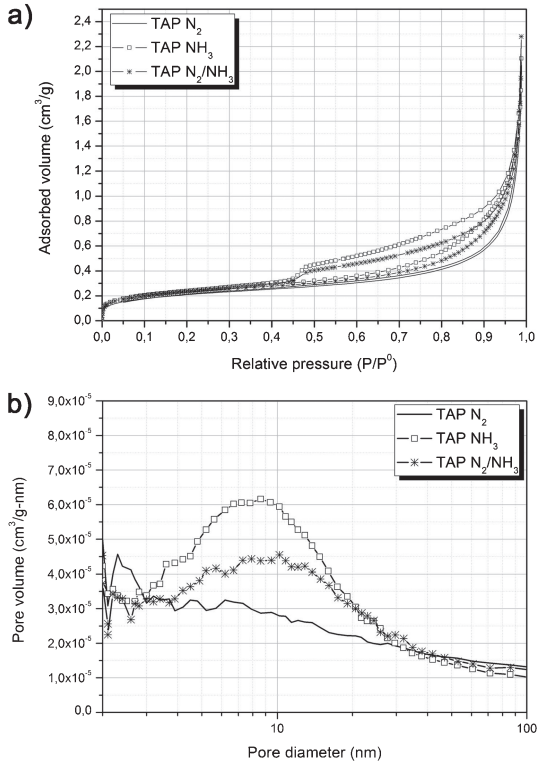

Fig. 3. a) Nitrogen adsorption isotherms of the TAP samples with 3% γ-APS heat treated in different atmospheres and b) the corresponding BJH pore size distributions.

allowing the Hg-liquid to penetrate within the material and then, not only the larger pores were analyzed but also the small ones. Breakage of the pore walls does not occur in the N_2 adsorption experiments.

In the case of the materials from the TAP system, it is observed a narrow PSD in all the cases, with pores sized around 1 µm [Fig. 1(b)]. The intruded volume is much lower than in the case of the TA samples and so does the differential pore volume. SEM images (Fig. 2) show a pore structure composed by tightly packed quasi spheres where the porosity is created by the inter-spatial voids between spheres contrary to the samples from the TA system showing a foam-like microstructure with closed porosity, not appreciable in the nitrogen adsorption measurements.

During pyrolysis, transient microporosity is generated at 800–1000 K in the materials from the system TAP but the materials remain macroporous in the system TA. This microporosity is absent in the materials pyrolyzed at 1373 K, as deduced from the N_2 adsorption measurements. Neither the ammonolysis nor the combined treatment origin new pores in the TA samples but some mesopores are observed in TAP samples (**Fig. 3**). As occurred in the TA system, the samples in TAP present increased mesopore volume in the samples heat treated under N_2/NH_3 and NH_3. Some authors have been reported the synthesis of stable microporous oxycarbonitride ceramics through ammonolysis of a polycarbosilane polymer where the micropores seem to be formed at the intermediate steps of the heat treatment by the creation of more robust units composed by Si–N–Si and Si–C–Si bonds rather than siloxane counterparts.[14] In the TAP system, the transient porosity created during pyrolysis may be reinforced in Si–N and Si–C units and thus be also the responsible of the retention of some mesopores at thermolysis temperatures above 1373 K.

In order to establish the evolution of the hybrid preceramic structure during the pyrolytic process and to identify the possible reactions involved in the hybrid to ceramic conversion, the structural characteristics of the two preceramic systems when heat treated in inert atmosphere has been followed through infrared spectroscopy. The progressive disappearance of the bands corresponding to the organic functionalities in the preceramic hybrids together with the enhancement of the bands corresponding to siloxane bonds are the main characteristics of the spectra.

In the system TA it was detected the increase of the band corresponding to borosiloxane bridges (674 cm^{-1}) but also the disappearance of the bands assigned to precipitates of H_3BO_3 coming from the hydrolyzed TEB alkoxide at the initial stages of the ceramic conversion. In the TAP system, the main feature is the shift to higher wavenumbers of the copolymerization band (D and Q units from PDMS and TEOS, respectively) centered at 850 cm^{-1} and the significant decrease of the band located around 1406 cm^{-1} and corresponding to B–O stretching. A common characteristic in the two systems is the appearance of the band attributed to methylene bridges (1277 cm^{-1}) at pyrolysis temperatures between 800–1000 K[19] and at 2264 cm^{-1} the band corresponding to O_3SiH bonds.[20] This former signal is still present at 1173 K but disappears when the pyrolysis temperature increases. This temperature was selected for switching atmospheres in the combined pyrolysis-ammonolysis treatment.

With regard to the structural characteristics of the heat-treated materials, the main feature of the infrared spectra of the TA materials is the well definition of the absorption bands as compared to the typical spectra of the polymer-derived-ceramics with broad bands such as those obtained in the TAP system (**Fig. 4**). All spectra were analyzed and deconvoluted to extract the relative intensity [with respect to the νs(Si–O–Si) band] and exact position of each band, a challenging task in the case of the system TAP because of the broadness of the bands. After the treatment in NH_3 atmosphere, the bands become broader because of the imposed disorder due to the incorporation of nitrogen into the network.

The band appearing at 674 cm^{-1} is attributed to the borosiloxane bending that, together with the band centered at 880 cm^{-1} assigned to the stretching mode of this Si–O–B bond, confirm the presence of these mixed units.[9] In the TA system, the bands assigned to borosiloxane bridges (674 cm^{-1}) remain with similar intensities in the three different treatments. However, the band associated with the vibration of the Si–X bonds (X = C, O, N) is centered at about 819 cm^{-1} and shifts to 824 cm^{-1} after the ammonolysis and pyrolysis-ammonolysis processes. In the system TAP, the band attributed to these species is centered at 816 cm^{-1} and exhibits a downshift in the case of the combined N_2/NH_3 process and even to a lower wavelength when the samples have been exposed exclusively to the ammonolysis treatment. The partial rupture of Si–O bonds to the formation the silicon oxycarbonitride network provokes the shift of the stretching band in the silicon tetrahedral towards smaller wavenumbers.[21] Nevertheless, the relative intensity of this band depends upon the concentration of γ-APS in the starting material. In both cases, it was observed a slight increase of the Si–X units with increasing amounts of γ-APS when the heat treatments were carried out in NH_3 or N_2/NH_3 atmospheres [Fig. 4(c)].

The ^{29}Si NMR spectra of the samples heat treated at 1373 K under different atmospheres are shown in **Fig. 5**. The spectra are very noisy, especially in those specimens heat treated in NH_3 atmosphere. The Gaussian deconvolution allows distinguishing between the different signals attributed to the multiple chemical

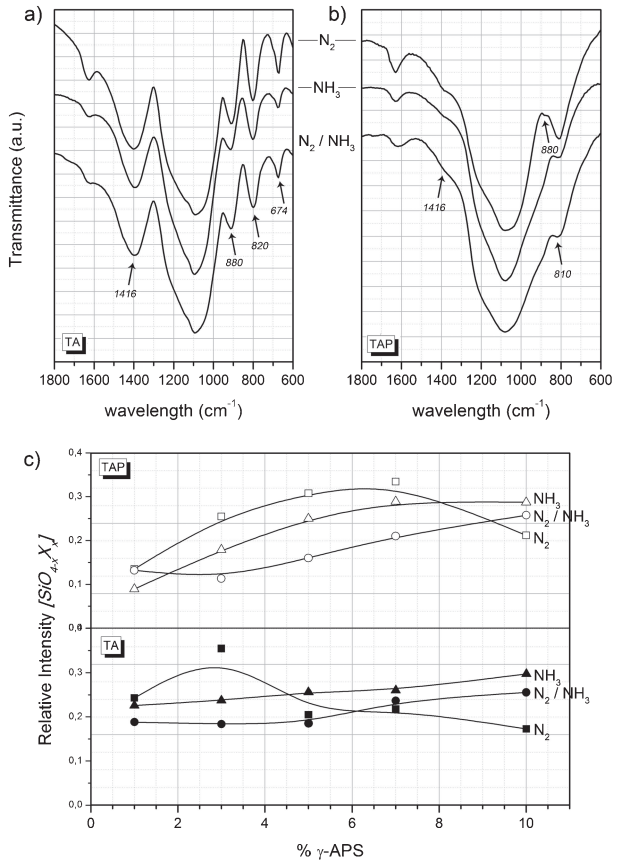

Fig. 4. Infrared spectra of a) TA and b) TAP materials containing 3% γ-APS and c) relative intensity of the band centered around 810 cm^{-1} and corresponding to Si–X (X = C, O, N) units.

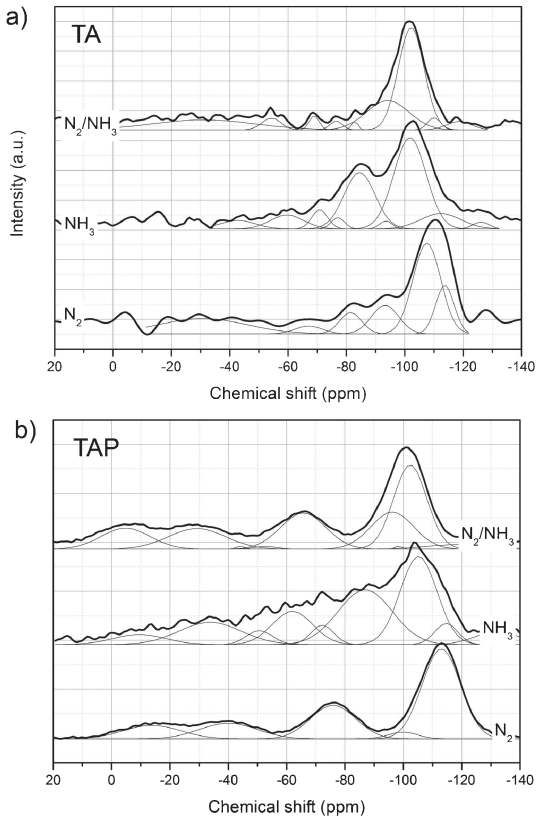

Fig. 5. ^{29}Si NMR spectra of a) TA and b) TAP materials containing 3% γ-APS and their convoluted bands.

environments in each material. Thus, the signal attributed to Q^4 environments appears centered around −110 ppm in all the samples and the signal at −100 ppm is assigned to Q^3 environments, which may correspond to some uncondensed silica species. The residual hydrogen detected in the chemical analyses (Table 1) might saturate some of the silanol groups giving as a result this lack of full condensation of the silica nodes.

The signal attributed to $[SiCO_3]$ species appears in the spectra at about −70 ppm but it is absent in the samples of the TAP system subjected to the treatment in the combined N_2/NH_3 atmosphere. Similarly, the signal due to $[SiC_2O_2]$ environments appears at −30 ppm in all the samples subjected to pyrolysis treatment, either alone or combined with ammonolysis.

The sum of the band intensities corresponding to $[SiO_{4-x}C_x]$ environments is higher in the case of the pyrolyzed materials and lower in the ammonolyzed samples, as may correspond to the partial substitution of C by N as a consequence of NH_3 in the treating atmosphere. Between the two studied systems, a large amount of C-enriched species can be found in the TAP materials, as it might be deduced from the chemical analysis.

The signal located at −90 ppm corresponds to $[SiNO_3]$ environments and is present in all the materials treated in NH_3 but the substitution of two oxygen atoms by nitrogen is only tentative in the samples from the TA system. Schitco et al.[14] assigned the signal appearing at about −83 ppm to $[SiO_2N_2]$ units in silicon oxycarbonitrides synthesized from preceramic polymers heat treated in an NH_3 atmosphere whereas the simulation of ^{29}Si NMR spectra of silicon nanoparticles suggest that this feature might be due to Si–H containing moieties, especially $[(Si–O)_3Si–H]$.[22] The absence of nitrogen in the pyrolyzed samples and the sharpness of the IR band assigned to borosiloxane bonds in the TA system [Fig. 4(a)] may be an indicative of the presence of these hydrogenated species since the bending mode of the Si–H bond is usually present as a narrow band at this precisely wavelength.[23] In the case of the ammonolyzed materials or heat treated in a combined N_2/NH_3 atmosphere, we cannot definitely assign the origin of this band and it could be a contribution either of the $[SiO_2N_2]$ units or Si–H bonds.

The substitution of O atoms by either C and N atoms can be found at the lowest chemical shifts and their convoluted bands are more clearly observed in the system TAP than in TA. After the ammonolysis treatment, the peak attributed to mixed environments, with both C and N attached to Si atoms such as $[SiCN_3]$ is found at around −45 ppm. The number of these species is larger than after the combined treatment in the system TA whereas in the TAP system, a new signal at above −52 ppm could be attributed to $[SiCNO_2]$ species. In TAP, at above −9 and −6 ppm in the case of NH_3 and N_2/NH_3 treatments respectively, the signal in the spectra was assigned to $[SiC_2N_2]$ environments, increasing in intensity in the case of the combined treatment. The sum of the intensities of all these species with at least two substituents of the Si tetrahedral are C and N is larger in the combined NH_3/N_2 treatment than after the direct treatment in NH_3. The major amount of mixed bonds either with C, N or both is indicative of more crosslinked networks than in the pyrolyzed samples.

The Raman spectra present the characteristic features of carbon-containing materials (**Fig. 6**) with the G band at 1570 cm^{-1} and the D band, at 1340 cm^{-1}. This band significantly broadens and shifts to 1330 cm^{-1} in the TAP materials, as correspond to C

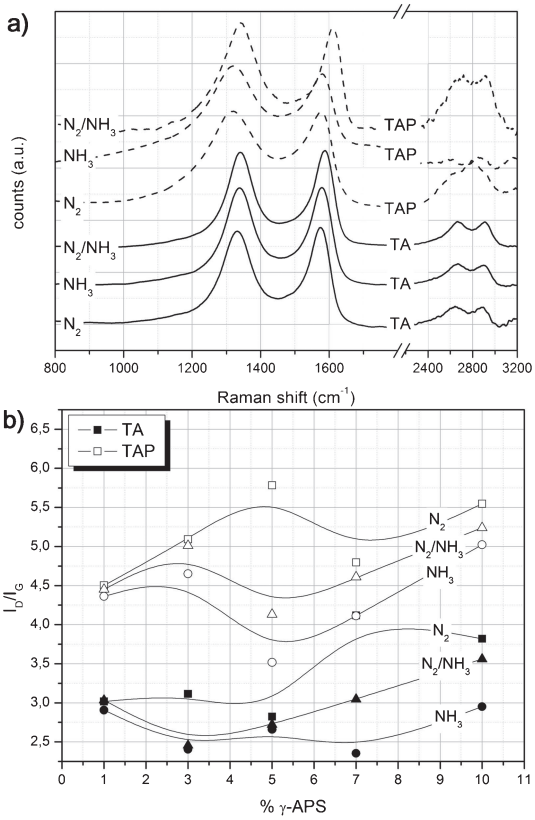

Fig. 6. a) Raman spectra of TA and TAP materials containing 3% γ-APS and b) relative intensity of the D and G bands as a function of the amount of γ-APS in the preceramic hybrid (solid lines are drawn to guide the eyes).

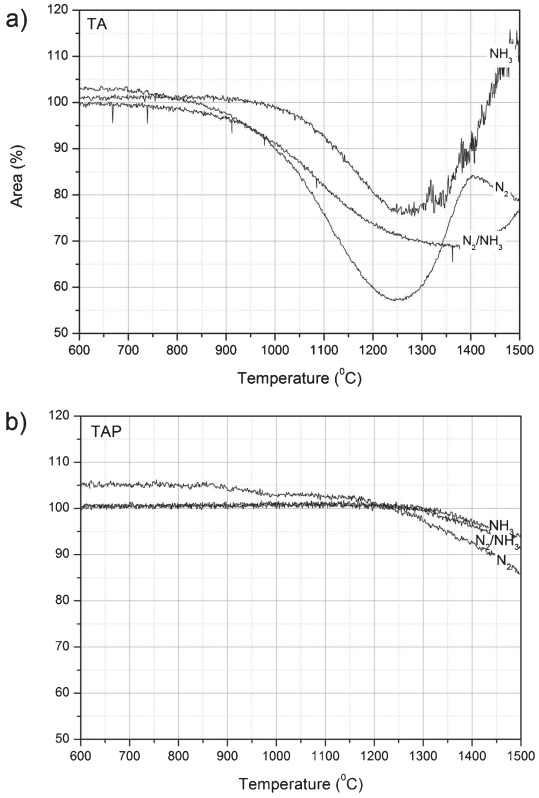

Fig. 7. Dimensional changes occurring in powdered test specimens obtained from the analysis of hot stage microscopy images in samples with 3% γ-APS from the system a) TA and b)TAP and heat treated in the different atmospheres.

clusters with ring ordering other than six.[24] The D′ band, appearing at above 1600 cm^{-1}, also moves to higher Raman shifts in the samples subjected to the combined treatment in both systems. The splitting of the G band into two peaks (G and D′) is associated to interactions between the localized vibrational modes of impurities or defects in the graphene layers with the extended phonon modes of pure sp^2 carbon[25),26] and, in the samples heat treated in N_2/NH_3, the enhancement of this D′ band may be attributed to a different redistribution path due to the atmosphere change at high temperature.

The relative intensity of D and G bands [I_D/I_G ratio, as shown in Fig. 6(b)] accounts for the degree of disordering in the free carbon phase and, in the studied materials, the general trend is an increase of the I_D/I_G ratio with the amount of γ-APS showing higher values in the materials from the TAP system than TA.

It is noteworthy the decrease in the intensity of the second-order Raman spectrum in the ammonolyzed samples, especially noticed in TAP materials. This second order Raman spectrum is most sensitive to the graphitization process leading to the three dimensional ordering of graphite-like clusters.[27] The disappearance of this second order bands is due to the loss of three dimensional ordering in the ammonolyzed samples,[24] as can be confirmed by the minor I_D/I_G ratio with respect to other heat treatments carried out in N_2 atmosphere. In both systems, the I_D/I_G ratio evolves along with the decrease of the B amount in the obtained material, indicating the major affinity of the B and N atoms. Peña-Alonso et al.[7] described the presence of highly graphitized carbon clusters promoted by boron atoms and in the works published by Chen et al.[11] it is described the formation of a hexagonal BN phase in SiBCN derived from borosilazane precursors heat treated at pyrolysis temperatures above 1673 K. Since the ammonolysis temperature used for the synthesis of SiBNCO materials is not high enough to promote the crystallization of BN crystals, the most plausible cause for the observed decrease in the three dimensional ordering of the free carbon phase in our ammonolyzed materials is the formation of mixed (B)CN bonds.

Hot stage microscopy (HSM) curves of the two studied systems present significant differences as reflected in **Fig. 7**. In the TA system, the samples retain their shape until 1033 K in the case of the materials treated in N_2, 1143 K in the ammonolyzed ones and 973 K in the materials heat treated in the combined treatment. Afterwards, the observed shrinkage attributed to powder sintering reaches its minimum value at 1523 K in both the pyrolyzed and ammonolyzed samples, with the area of the test specimens being 56 and 76% lower with respect to that of the preceramic samples, respectively. In the case of the sample subjected to the combined treatment, sintering occurs more progressively ending at 1673 K where the area of the specimen is reduced by 30%. After sintering, in all the cases it is observed the expansion of the test areas probably due to incipient nucleation of crystalline species. Only in the pyrolyzed sample a new shrinkage step is detected at temperatures above 1673 K. In the system TAP the area of the test specimen subjected to a pyrolysis treatment experiments a gradual decrease of about 1% in the temperature range comprised between 1253 and 1428 K and afterwards the area of the sample is reduced at a high rate due to the sintering of the powders. At the end of the experiment, the final area of the

sample is 86% with respect to the original area. The samples heat treated in NH_3 and N_2/NH_3 atmospheres follow the same path starting the sintering of the powders at 1573 K.

The observed behavior in the HSM experiments is well correlated with the structural characteristics of each system. In the system TA, the highly macroporous SiBOC network formed during pyrolysis is prone to early sintering at low temperatures. Treatment in NH_3 atmosphere produces an increase of the network stiffness due to the formation of mixed SiCN bonds. The delayed crystallization temperature in the combined N_2/NH_3 treatment is attributed to a thick BCN layer that restricts the mobility of the atoms to form the crystalline species. On the other hand, the system TAP only presents a small amount of mesopores mainly composed by Si–N–Si and Si–C–Si bonds, a fact that significantly delays the softening temperature of these materials.

4. Conclusions

The formation of a SiBCO(N) network is confirmed through spectroscopic characterization of the obtained materials. The infrared analysis revealed the presence of the signals attributed to borosiloxane bridges (880 and 674 cm^{-1}) and Si–X (X = O, C, N) species (816–824 cm^{-1}). The shift of the bending mode of Si–O bonds (typically centered below 800 cm^{-1}) is attributable to the substitution of the O atoms either by C or N. In both systems, the slight increase in the amount of these Si–X units with increasing amounts of γ-APS when the heat treatments were carried out in NH_3 or N_2/NH_3 atmospheres suggests a more crosslinked structure. ^{29}Si NMR analysis shows that after the ammonolysis treatment, the amount of Si–C enriched species decreases significantly in both systems because of the reaction of C-containing moieties with NH_3 promoting the formation of Si–N bonds. The presence of $[SiNO_3]$ units is found in both systems subjected to any treatment involving NH_3 but not $[SiCO_3]$ structural units, which are absent in the TAP materials. These $[SiCO_3]$ species are the most reactive against the substitution of N by C atoms. The combined pyrolysis-ammonolysis treatment leads to an increase of the $[SiCN_3]$ structural units in both systems, but it is especially remarkable in the system TA. The replacement of O by C and N such as in $[SiCNO_2]$ structural units is a remarkable feature of the TAP system when heat treated in the combined N_2/NH_3 treatment. The low-B-content system TAP presents some $[SiC_2N_2]$ species whose appearance is more emphasized in the case of the combined N_2/NH_3 treatment. To conclude, ammonolysis leads to less graphitized materials with low 3D ordering, as described in the Raman analysis. The combined pyrolysis-ammonolysis method has been proved as a convenient heating treatment to prevent the loss of C during the treatment in a single NH_3 atmosphere Switching the atmosphere from N_2 to NH_3/N_2 at the temperature where the C clusters starts to appear leads to a major retaining of the C atoms in the Si(B)OCN network due to the formation of more reactive species against NH_3 at these stages.

Acknowledgments Financial support by Fundación General CSIC (Programa ComFuturo) is acknowledged.

References

1) E. Ionescu, H.-J. Kleebe and R. Riedel, *Chem. Soc. Rev.*, 41, 5032–5052 (2012).
2) P. Greil, *Adv. Eng. Mater.*, 2, 339–348 (2000).
3) A. Tamayo, M. A. Mazo, F. Rubio and J. Rubio, *Ceram. Int.*, 40[7, Part B], 11351–11358 (2014).
4) V. Ischenko, E. Pippel, J. Woltersdorf, B. R. N. Yappi, R. Hauser, C. Fasel, R. Riedel, F. Poli and K. Muller, *Chem. Mater.*, 20, 7148–7156 (2008).
5) M. N. Muralidharan, N. C. Pramanik, P. A. Abraham, K. Stanly Jacob and N. Rani Panicker, *Mater. Lett.*, 62, 2547–2550 (2008).
6) L. J. Yang, Y. Zhang and X. Cheng, *Progress in Chemistry*, 28, 308–316 (2016).
7) R. Pena-Alonso, G. Mariotto, C. Gervais, F. Babonneau and G. D. Soraru, *Chem. Mater.*, 19, 5694–5702 (2007).
8) Y. Jiang, J. Li, F. Huang, Y. Zhou and L. Du, *J. Am. Ceram. Soc.*, 97, 310–315 (2014).
9) M. A. Schiavon, C. Gervais, F. Babonneau and G. D. Soraru, *J. Am. Ceram. Soc.*, 87, 203–208 (2004).
10) A. H. Tavakoli, P. Gerstel, J. A. Golczewski and J. Bill, *J. Mater. Res.*, 26, 600–608 (2011).
11) Y. Chen, X. Yang, Y. Cao and L. An, *J. Eur. Ceram. Soc.*, 34, 2163–2167 (2014).
12) B. Tang, Y. Zhang, S. Hu and B. Feng, *Ceram. Int.*, 42, 5238–5244 (2016).
13) L. Gottardo, S. Bernard, C. Gervais, M. Weinmann and P. Miele, *J. Mater. Chem.*, 22, 17923–17933 (2012).
14) C. Schitco, C. Turdean-Ionescu, M. S. Bazarjani, C.-W. Tai, D. Li, C. Fasel, W. Donner, J. Shen, R. Riedel, A. Gurlo and M. Eden, *J. Eur. Ceram. Soc.*, 36, 979–989 (2016).
15) N. S. Choong Kwet Yive, R. J. P. Corriu, D. Leclercq, P. H. Mutin and A. Vioux, *Chem. Mater.*, 4, 141–146 (1992).
16) S. Duperrier, C. Gervais, S. Bernard, D. Cornu, F. Babonneau and P. Miele, *J. Mater. Chem.*, 16, 3126–3138 (2006).
17) C. J. Brinker, D. M. Haaland and R. E. Loehman, *J. Non-Cryst. Solids*, 56, 179–184 (1983).
18) O. Vollmer, F. d. r. Lefebvre and J. S. Bradley, *J. Mol. Catal. A: Chem.*, 146, 87–96 (1999).
19) R. Peña-Alonso, F. Rubio, J. Rubio and J. L. Oteo, *J. Anal. Appl. Pyrolysis*, 71, 827–845 (2004).
20) K. W. Jobson, J. P. R. Wells, N. Q. Vinh, P. J. Phillips, C. R. Pidgeon and J. I. Dijkhuis, *Opt. Mater.*, 30, 740–742 (2008).
21) N. I. Fainer, A. G. Plekhanov, Y. M. Rumyantsev, E. A. Maximovskii, V. R. Shayapov, A. G. Plekhanov, Y. M. Rumyantsev, E. A. Maximovskii and V. R. Shayapov, *Glass Phys. Chem.*, 40, 570–577 (2014).
22) R. Faulkner, J. DiVerdi, Y. Yang, T. Kobayashi and G. Maciel, *Materials*, 6, 18–46 (2013).
23) D. J. Michalak, S. R. Amy, D. Aureau, M. Dai, A. Esteve and Y. J. Chabal, *Nat. Mater.*, 9, 266–271 (2010).
24) A. C. Ferrari and J. Robertson, *Phys. Rev. B*, 61, 14095–14107 (2000).
25) N. Larouche and B. L. Stansfield, *Carbon*, 48, 620–629 (2010).
26) A. C. Ferrari and D. M. Basko, *Nat Nano*, 8, 235–246 (2013).
27) P. Lespade, R. Aljishi and M. S. Dresselhaus, *Carbon*, 20, 427–431 (1982).